22. Interglacial and Glacial Fingerprints from Lake Deposits in the Gobi Desert, NW China

Bernd Wünnemann[1], Kai Hartmann[2], Norbert Altmann[2], Ulrich Hambach[3], Hans-Joachim Pachur[2] and Hucai Zhang[4]

[1]Interdisciplinary Centre Ecosystem Dynamics in Central Asia, Freie Universitaet Berlin, Malteserstr. 74-100, 12249 Berlin, Germany
[2]Institut für Geographische Wissenschaften, Freie Universitaet Berlin, Malteserstr. 74-100, 12249 Berlin, Germany
[3]Lehrstuhl für Geomorphologie, Universitaet Bayreuth, Universitaetsstr. 3, 95447 Bayreuth, Germany
[4]Nanjing Institute of Geography and Limnology (NIGLAS), Chinese Academy of Sciences, China

ABSTRACT

A 230-m long sediment core from the centre of the Gaxun Nur Basin, Gobi Desert, NW China provides evidence for climate induced changes in water balance during the last glacial cycle. Millennial scale and short-term variations of geochemical precipitates and grain size show that freshwater fluxes from the Tibetan Plateau by surface run-off were the main controlling factors for lake evolution in the Tibetan dry forelands for about the last 250 kyr. Periods of positive water balance with strong lake extension and reverse developments generally coincide with changes in the global ice volume and with oxygen-18 records from Tibet and Greenland as well, documenting the close relationship between environmental conditions in remote desert regions of NW China and orbitally forced Northern Hemisphere high mountain mid-latitude and high-latitude climates on a regional and global scale. Our data imply that both the East Asian summer monsoon and the extra-tropical westerlies are the major feedback mechanisms for effective moisture supply over NW China.

During the 10-kyr long interglacial warm-moist substage 5.5, summer monsoon moisture dominated owing to its strong northward shift beyond the modern limit. At that time, a large and slightly saline lake filled the entire Gaxun Nur basin as a result of strong river inflow from the Tibetan catchment by melt water supply and by enhanced summer monsoon precipitation.

Aeolian transport was weak. The Eemian interglacial in the Gaxun Nur region started at about 129 kyr, with warm and moist environmental conditions between 128 and 121 kyr BP and terminated around 119 kyr, documented by a strong climate shift towards dry conditions and enhanced mobilization of aeolian sand.

During interstadial climates, contemporaneous with D/O events in Greenland ice cores, both wind systems most likely supplemented each other, while in transitional phases towards cold conditions, moisture supply by the westerlies seems to have dominated. Cold-dry stages, recorded in the Gaxun Nur core, are synchronous with the global climate. They induced strong lake-level declines and promoted aeolian transport of exposed lake sediments southwards due to the enhanced winter monsoon. Loess records from the Chinese Loess Plateau confirm that the temporal distribution of loess mobilization recorded in the Gaxun Nur sediments was synchronous with depositional phases on the Loess Plateau.

22.1 INTRODUCTION

Rapid climate fluctuations during the last glacial cycle are well documented in ice cores from Greenland (e.g. Dansgaard *et al.*, 1993; NorthGRIP Project Members, 2004) and from Antarctica (Petit *et al.*, 1999), the latter tracing back to the last eight cycles during Quaternary time (EPICA Members, 2004). They obviously have played a major role in reconstructing climate changes. Although it is widely accepted that the main driving force of climate shifts in orbital bands is strongly related to solar radiation (insolation) through time (e.g. Berger and Loutre, 1991; Clement *et al.*, 2001; Leuschner and Sirocko, 2003), feedback mechanisms such as inland ice dynamics, thermohaline circulation and the atmospheric circulation pattern (e.g. the Northern Hemisphere low- and mid-latitude monsoon systems) may have affected land–ocean thermodynamic relations quite differently at regional scales. In particular, the climates over Asia seem to have been strongly influenced by the uplift of the Tibetan Plateau (An *et al.*, 2001), co-controlling the evolution of the Asian monsoon system and the establishment of the Inner Asian dryland belt (Gobi Desert). However, palaeoclimate studies reveal the general high–frequency climate instability during the last glacial cycle, well known from Greenland ice cores and from North Atlantic sediment cores as stadials (Bond cycles and Heinrich events) and interstadials (Dansgaard–Oeschger cycles) on timescales of a few millennia (e.g. Dansgaard *et al.*, 1993; Bond *et al.*, 1997). The recognition of those climate cycles in marine sediments of the Arabian Sea (Schultz *et al.*, 1998; Leuschner and Sirocko, 2003), South China Sea (e.g. Wang *et al.*, 1999), in ice cores from Tibet (Thompson *et al.*, 1997; Thompson, 2000) and in aeolian sediments from the Chinese Loess Plateau (e.g. Porter and An, 1995; Xiao *et al.*, 1995) confirms a close relationship between low-latitude monsoonal climate variability and rapid temperature fluctuations of higher northern latitudes (e.g. Schulz *et al.*, 1998). A linkage between the Tibetan uplift, monsoon pattern and Northern Hemisphere glaciation seems to be evident (An, 2000; An *et al.*, 2001).

On the other hand, very little is known about feedback mechanisms controlling the expansion or shrinkage of arid regions in inner Asia during interglacial and glacial cycles and which of them might be dominant. The special significance of this dryland belt in strongly continental China north of the Tibetan Plateau with respect to climate reconstructions is due to the fact that two different northern hemispheric air masses – the East Asian Monsoon and the extra-tropical westerlies – intersect in this region. Both wind regimes are potential sources for water vapour transport, affecting the regional hydrological systems on the Tibetan Plateau and the desert forelands. Alternations in the summer monsoon strength as one prominent source of water vapour transport from low latitudes into the interior of China seem to have responded synchronously to major shifts in the climate system on a global scale, but on a regional scale the monsoonal effect varied considerably (An *et al.*, 2001). At present, nearly nothing is known about the potential impact of the westerlies system, either compensating the lack of moisture transport by the monsoon system or even enhancing moisture availability along the arid zones of Central Asia.

Previous palaeoclimate studies have shown that vast desert areas in north-western China were covered by large lakes and swamps during marine isotope stage 3 (MIS) and during early and mid-Holocene times (Pachur *et al.*, 1995; Wünnemann *et al.*, 1998; Zhang *et al.*, 2001, 2002, 2004; Wünnemann and Hartmann, 2002; Mischke *et al.*, 2005) as a result of enhanced local precipitation and melt water discharge in periods of glacier advance in the high mountain catchments. All climate proxies in that region trace back to approximately 40 kyr. Here we present a sediment record from the Gaxun Nur Basin in arid north-western

China which is assumed to cover the sedimentary history of the past 250 kyr. However, we focus on climate-controlled hydrological changes during the last glacial cycle. In this paper, we try to answer the questions (i) whether the water balance of the Gaxun Nur system reflects climate shifts from warm to cold stages and vice versa synchronously with global climate signatures and (ii) whether phases of aeolian activity respond to variations in the wind regime over NW China.

22.2 GEOLOGICAL SETTING

The Gaxun Nur Basin – part of the Alashan Plateau – forms an intramontane accumulation area between the Qilian mountains in the south and Gobi Altai mountains in the north (Fig. 22.1). Both mountain ranges are influenced by left-lateral plate motions accompanied by intense vertical displacements due to the ongoing collision of the Indian plate against the Eurasian continent. The sinistral pattern continues northwards from the Qilian Mts. via the Hexi Corridor (Gansu Corridor, better known as a part of the former Silk Road) towards the Alashan Plateau (Molnar and Taponnier, 1975; Li *et al.*, 1999; Hetzel *et al.*, 2002; Hartmann, 2003), thus forming the 'belt of left-lateral transpression' (Cunningham *et al.*, 1996). Consequently, the Gaxun Nur Basin developed as a large pull-apart-basin between these structural elements, now acting as the erosional base for the Hei River drainage system from the south (Tibetan Plateau). This endorheic basin covers an area of approximately 28 000 km^2, while the total catchment of the Hei River system, connected with glaciers in the Qilian Mts., comprises roughly 130 000 km^2. Along the distal part of the basin, three terminal lakes – Gaxun Nur, Sogo Nur and Juyanze – form a sickle-shaped chain. At present, all lakes are dry.

At present, climate in NW China is mainly controlled by the East Asian Monsoon transporting effective moisture during summer time up to its northern limit at about 40°N, parallel to the Yellow River course outside the Tibetan Plateau, and

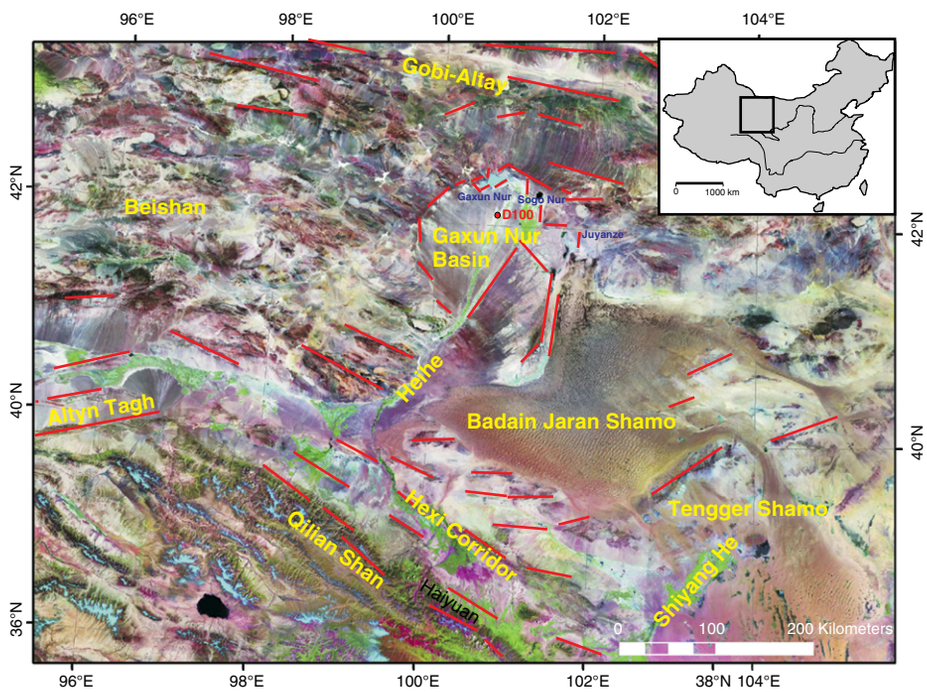

Fig. 22.1 Satellite image (RGB 7-4-2) of the Gaxun Nur Basin north of the Tibetan Plateau with location of the deep drilling D100 and major structural elements (red lines correspond to faults).

intersecting with the westerly waves, generating local rainfall as well as heavy rainfall events by overlying air masses of different temperature and water vapour content during summer time (Domrös and Peng, 1988). The intensity of summer rainfall strongly depends on the pressure gradient between the heat low over Tibet and the anticyclone over the Pacific ocean, resulting in highly variable annual precipitation between <40 mm and roughly 100 mm within the desert regions, while in the upper catchment of the Hei River precipitation rises to 500 mm/year. The annual amplitude of monthly mean temperatures ranges between 28°C in summer and −12°C in wintertime. During wintertime, cold dry air masses from the anticyclone over Siberia are responsible for extremely low temperatures and strong winds from northern directions without appreciable precipitation. Owing to the southward shift of the westerlies in wintertime, rain or snowfall from that source is negligible. According to the distribution of annual precipitation, river discharges towards the Gaxun Nur Basin peak during spring and late summer.

Owing to strong human impact, e.g. water storage in the upper reaches of the Hei River for irrigation purposes, the terminal lakes Gaxun Nur and Sogo Nur have desiccated since the 1960s, while the hydrologically separated Juyanze Lake dried up much earlier during the Han Dynasty (third century AD).

Besides the well-developed drainage pattern of south–north-directed river channels, a dense network of presently dry channel systems originates north of the basin and indicates strong fluvial input from the Gobi Altai ranges mainly developed during early and mid-Holocene wet periods (Wünnemann, 1999; Hartmann, 2003). They required much more local rainfall than the present amount.

Previous investigations by Wünnemann and Hartmann (2002) indicate an extended paludine environment of $>10\,000\,km^2$ in size during MIS 3 between 35 and 25 kyr, evidenced by the distribution of dated near-surface lake sediments and palaeoshorelines of up to 25 m above the present dry lake floors at 900 m above sea level.

The up to 300-m thick basin fills of Quaternary age are documented by a total of 80 drillings (Gansu Provincial Geological Bureau, 1980). The dominant facies is of lacustrine origin with grain-size diameters in the clay and silt fractions, locally interrupted by fluvial and aeolian sand. Coarse gravels were found only in the upper metres of some cores. During the terminal phase of the last glacial maximum (LGM) and most probably during early Holocene times, strong fluvial run-off promoted the accumulation of fluvial sand and coarse gravels from local catchment sources and covered large areas of the basin, protecting the fine-grained lacustrine sediments against deflation. However, according to Pye and Zhou (1989), this region still serves as a prominent source area for loess transport.

Recently published results by Hartmann (2003) and Becken *et al.* (2003) indicate a very young tectonically induced subsidence of the northern part of the basin by about 2 mm/yr during the last 30 kyr. In terms of hydrology, the three terminal lakes have been separated since then. This would explain the differences in sedimentation behaviour between the Gaxun Nur system and the eastern palaeolake Juyanze during Holocene time as suggested by Hartmann (2003). However, previously reported highest lake levels of the Gaxun Nur system during MIS 3 (Pachur *et al.*, 1995; Wünnemann and Hartmann, 2002) developed prior to these tectonic events. Hence, the sediment core D100, retrieved from a deep drilling in the centre of the Gaxun Nur Basin, remains suitable for climate reconstructions.

22.3 METHODS

For the coring of D100 sediments, we used a Chinese rotational drilling system with 3 m long metal tubes 80–120 mm diameter in

size. The drilling in the centre of the Gaxun Nur Basin at 42.1°N, 100.85°E, 940 m a.s.l. reached the pre-Quaternary sediments at 229 m depth. Once a core segment was retrieved, it was pressed out immediately, halved, described and finally documented by photographs. Sampling of 1-cm thick slices was done every 10 cm, depending on stratification. Where necessary, sampling was narrowed down to 1 cm, for example within laminated sequences. For analyses of micromorphological features, thin sections of selected samples were prepared and analysed under a polarization microscope.

Samples for magnetic properties were taken as cubes of 8 cm^3 size and measured in the laboratory for Palaeo- and Environmental Magnetism (PUM), Bayreuth University. All samples were subjected to standard palaeo- and rock magnetic laboratory protocols. However, here we focus on the inclination record of the characteristic remanent magnetization derived from the results of stepwise demagnetization in alternating magnetic fields. A record of the relative palaeointensity (RPI) of the Earth's magnetic could not be determined because of the pronounced rock magnetic heterogeneity of the sediments, which did not allow for a proper normalization of the intensity of the characteristic remanent magnetization. Thus, the stratigraphic interpretation is based on the correlation of our inclination data with the stacked record of RPI of the Earth's magnetic of Thouveny *et al.* (2004).

Dried and powdered samples for geochemical analyses were performed as follows:

- Total organic carbon (TOC) and CO_3 by loss on ignition (550 and 900°C) and by LECO carbon analyser (infrared spectrometry) following standard procedures.
- Multielement analyses of Ca, Mg, Fe, Mn, Na, K, S and PO_4 by a Perkin Elmer optical emission spectrometer with inductive coupled plasma (ICP-OES) on pretreated samples by hydrochloric acid (HCl) digestion.

The mineral compositions of selected samples were detected by XRD (Philips PW1710, Cu-cathode, 36 kV, 24 mA). Grain-size analyses were performed by a laser diffraction particle sizer (Beckman Coulter LS 200) after removal of carbonate and organic compounds by HCl and H_2O_2 treatment respectively. To avoid coagulation, sodium-pyro-phosphate ($Na_4P_2O_7 * 10H_2O$) was added, and the sample was then shaken for several hours. Before measurement, every sample was divided into eight subsamples and, where necessary, dispersed in an ultrasonic bath. At least three subsamples were measured in each case. Thus, the final grain-size distribution of each sample is based on the average of three subsamples.

Radiometric dating (AMS) on bulk samples was done at Leibniz Laboratory, Kiel, Germany, and Beta Analytics, Miami, USA. In several cases, twin dating of the organic carbon from the remaining lye fraction and humic acid was performed to estimate contamination within one sample. Additionally, thermoluminescence dating (IRSL, OSL) of sandy lake sediments was performed at the Geophysical Laboratories of the Chinese Academy of Science, Beijing, China, and at the Saxonian Academy of Sciences, Freiberg, Germany. Both laboratories used feldspar grains for dating.

22.4 AGE MODEL

For reconstructing changes in water balance of the Gaxun Nur Basin and variations in dust mobilization through time, several independent age determinations were performed. Unfortunately, previously reported radiocarbon and TL/IRSL ages from the D100 core between 11 and 90 m depth (Wünnemann, 1999; Table 22.1) do not correspond to OSL dates from a parallel core I70, but show age differences of several 10 000 years. According to geomorphological investigations and radiometric

Table 1 Absolute age determinations from the cores D100 and I70 (parallel core) and adjacent sites, Gaxun Nur Basin, NW China

Sample	Mean depth (m)	Laboratory number	Dated material	mg C	AMS age kyr	TL/IRSL/OSL age kyr	Deviation +	Deviation −	δ^{13}C (‰)
Core D100 Gaxun Nur (42.1 °N, 100.85 °E, 940 m a.s.l.)									
D100-1	9.35	Beij1	Lake sand			22	1.8	1.8	
D100-2	11.13	Hv20383	Bulk carbonate		21.265		0.5	0.5	−3.9
D100-1101	11.22	beta 188774	Bulk organic Carbon		14.45		0.1	0.1	−23.6
D100-1601	16.29	beta 189674	Bulk organic Carbon		14.29		0.1	0.1	−23
D100-IRSL1	16.46	Beij2	Lake sand			29.20	3.7	3.7	
D100-1901	19.71	beta 189675	Bulk organic Carbon		17.00		0.1	0.1	−22.9
D100-IRSL2	19.73	Beij3	Lake sand			41.10	2.9	2.9	
D100-IRSL3	22.27	Beij4	Lake sand			54.50	5.0	5.0	
D100-3402	34.50	beta 190783	Bulk organic Carbon		16.86		0.1	0.1	−23.2
D100-3904	40.06	beta 190784	Bulk organic Carbon		16.72		0.1	0.1	−22
D100-IRSL4	44.03	Beij5	Lake sand			90	6.2	6.2	
D100-10	44.22	KIA24208	Bulk organic Carbon	3.9	34.82		0.4	0.4	−25.03
D100-10	44.22	KIA24208	Humic acid	0.7	30.00		0.8	0.7	−25.02
D100-IRSL5	60.73	Beij6	Lake sand			196	15.0	15.0	
D100-11	65.59	KIA24209	Bulk organic Carbon	0.7	26.41		0.5	0.5	−22.86
D100-11	65.59	KIA24209	Humic acid	1	34.57		1.0	0.9	−23.86
D100-IRSL6	71.90	Beij7	Lake sand			202	17.0	17.0	
D100-12	72.25	KIA24848	Bulk organic Carbon	1.3	35.85		0.9	0.8	−22.78
D100-12	72.25	KIA24848	Humic acid	2.4	27.57		0.3	0.3	−21.55
D100-12	72.25	KIA24848	Bulk organic Carbon	0.4	23.75		0.7	0.6	−26.83
D100-13	76.99	KIA25440	Bulk organic Carbon	0.5	20.56		0.4	0.3	−25.14
D100-13	76.99	KIA25440	Humic acid	0.2	25.73		1.7	1.4	−30.77
D100-14	79.71	KIA25441	Humic acid	0.3	27.20		1.3	1.1	−27.08
D100-14	79.71	KIA25441	Bulk organic Carbon	0.9	25.64		0.4	0.4	−20.09
D100-15	90.12	KIA25756	Bulk carbonate	0.5	>41.52				−4.03
D100-8911	90.12	KIA25756	Bulk organic Carbon	1.6	30.71		0.4	0.4	−19.08
I70-16	11.77	Beta 188775	Bulk organic Carbon		8.89		0.08	0.08	−23.9
I70-1470	14.70	Freiberg	Lake sand			146	10	10	
I70-17	14.80	Beta 189676	Bulk organic Carbon		11.18		0.05	0.05	−21.1
I70-2900	29.0	Freiberg	Lake sand			172	12	12	
I70-18	29.67	Beta 190786	Bulk organic Carbon		6.97		0.06	0.06	−23.0
I70-3850	38.50	Freiberg	Lake sand			230	16	16	
I70-5050	50.50	Freiberg	Lake sand			281	23	23	
HC8 cliff	5.0	Beta 190785	Bulk organic Carbon		15.060		0.08	0.08	−22.8
96E27	4.0	KIA 23627	Bulk organic Carbon	0.4	17.390		0.25	0.25	−22.49
HC21	4.0	KIA 24143	Ostracod shell	0.9	22.790		0.15	0.15	−1.66

Locations of the last three dates, see Wünnemann and Hartmann (2002) and Hartmann (2003).

datings of palaeoshorelines and near-surface lake sediments of the Gaxun Nur system which revealed ages from the Holocene to Late Pleistocene MIS 3 (Wünnemann and Hartmann, 2002; Hartmann, 2003), all IRSL and OSL dates have to be considered too old. A series of AMS dates from the core D100 between 11 and 90 m depth revealed much younger ages (Table 22.1), roughly correspondent with age determinations in the closer catchment of the lake.

The AMS dates, however, do not increase with depth but scatter in a wide range between 20 and 40 kyr up to 90 m depth. Age differences between the remaining lye fraction and humic acid support the assumption of repeated reworking processes within phases of flooding during MIS 2 and 3, initiated by tectonically induced subsidence. As a result, extremely high redeposition of clastic material took place. Washing and sieving of bulk sediments for ostracod analyses revealed very few specimens of broken valves, thus confirming redepositional processes. This assumption is supported by the occurrence of wood remains >1000 µm in size and charcoal particles which have been transported by single flooding events from various locations. This might be the reason why the AMS dates scatter irregularly through depth.

Owing to uncertain absolute age determinations, we used palaeomagnetic datasets for further chronological approaches. Measurements from 65 to 156 m and from 187 to 198 m core depth revealed intervals with reverse inclinations at 67–93 m, 122–142 m and 190–196 m core depth respectively (Fig. 22.2). According to our AMS dates and to the palaeointensity record of Thouveny *et al.* (2004), the intervals with reverse inclinations of core D100 most likely correspond to relative lows of the Earth's magnetic dipole moment at about 25 to 45, 95 to 125 and 185 to 195 kyr containing the Laschamp, post Blake, Blake and Icelandic Basin geomagnetic events, thus giving the tie points for our chronology so far. As the

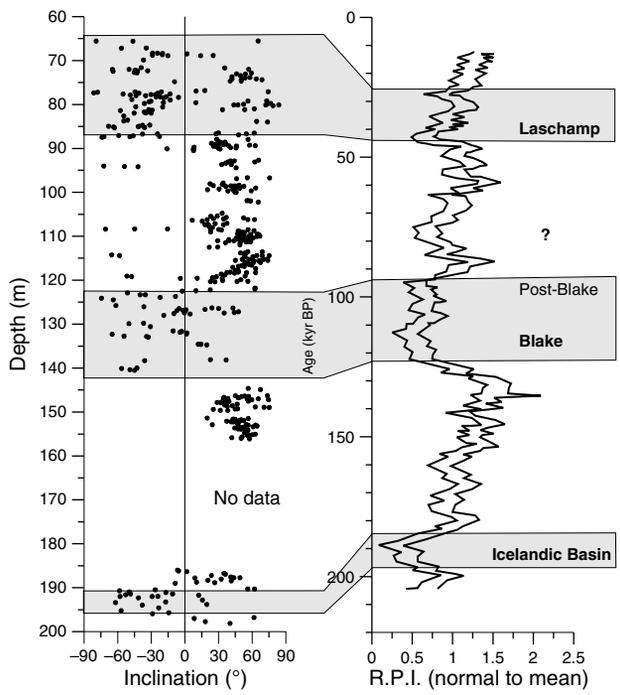

Fig. 22.2 Palaeomagnetic results from core D100 show intervals of reverse inclinations of the characteristic remanent magnetization at 67–93 m, 122–142 m and at 190.5–196 m depth. Comparisons with the stacked record of Thouveny et al. *(2004) indicate that the intervals with reverse inclinations in D100 core match the Laschamp, post-Blake, Blake and Icelandic Basin subchrones, hence giving major tie points for our chronology.*

lithology of the core from 71 m depth downward consists of more or less uniform rhythmic silt-clay layers, we calculated a linear sediment accumulation rate (SAR) of 7.1 cm/century (63–128 m depth, Fig. 22.3) and 6.8 cm/century (144–228 m depth) except for parts between 128 and 144 m depth, where intercalated sandy layers of aeolian origin required a higher SAR of 8.5 cm/century (Fig. 22.4). With respect to the Blake and post-Blake reverse inclinations at 142–123 m core depth, we calculated for the reversal peak at 140 m depth an age of 115 kyr, thus matching the lowest RPI in the record of Thouveny *et al.* (2004) and the reverse inclination in core MD95-2042 from the Portuguese margin as well (Thouveny *et al.*, 2004, Fig. 22.4b). Hence, the sediments

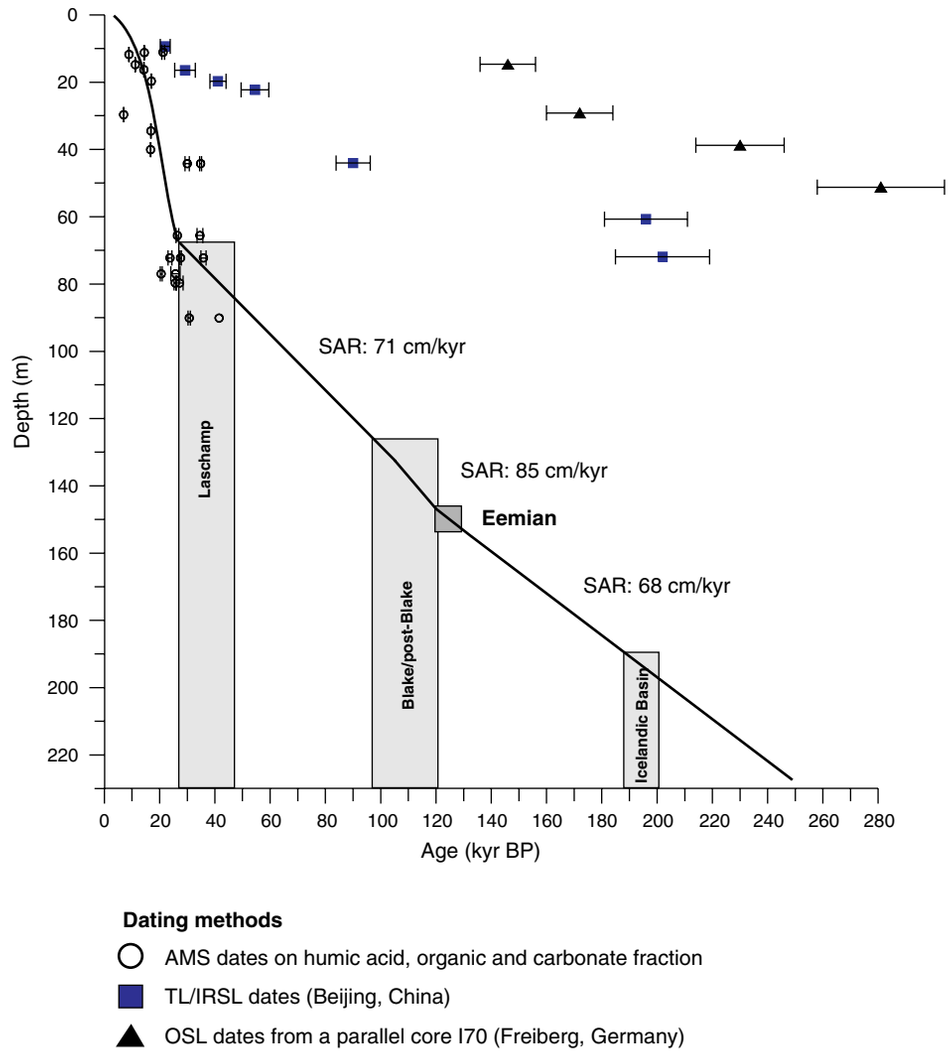

Fig. 22.3 The age–depth relation of the core D100 based on palaeomagnetic data and AMS dates. Our model indicates nearly constant sediment accumulation rates of lacustrine sediments from 71 m downwards, except for the sequences between 128 and 144 m depth. Thermoluminescence dates (IRSL and OSL) are not used for this chronology as they are considered to be too old and do not confirm geomorphological investigations.

of the entire core D100 probably comprise the sedimentary history of the past 250 kyr, a much shorter time than previously expected (Wünnemann and Hartmann, 2002).

22.5 RESULTS

22.5.1 Sediments of core D100, Gaxun Nur

The 230-m thick sediments from the centre of the Gaxun Nur Basin were retrieved by 110 cores of maximum 3 m length. Recovery reached about 78% of the whole sediment column. Missing parts are usually related to sandy sequences, difficult to retrieve by a rotational drilling technique without liners. However, strata with pelitic sediments had a coverage of nearly 100%. In general, the sediments of core D100 can be divided into three lithological units (Fig. 22.4A): gravels in the top 7 m, frequent alternations of sand and silt between 7 and 71.4 m depth and laminated clay-silt layers from 71.4 m downwards. The bottom sediments from 228.8 m to 230 m depth consist of pre-Quaternary red conglomerates in a clayey matrix.

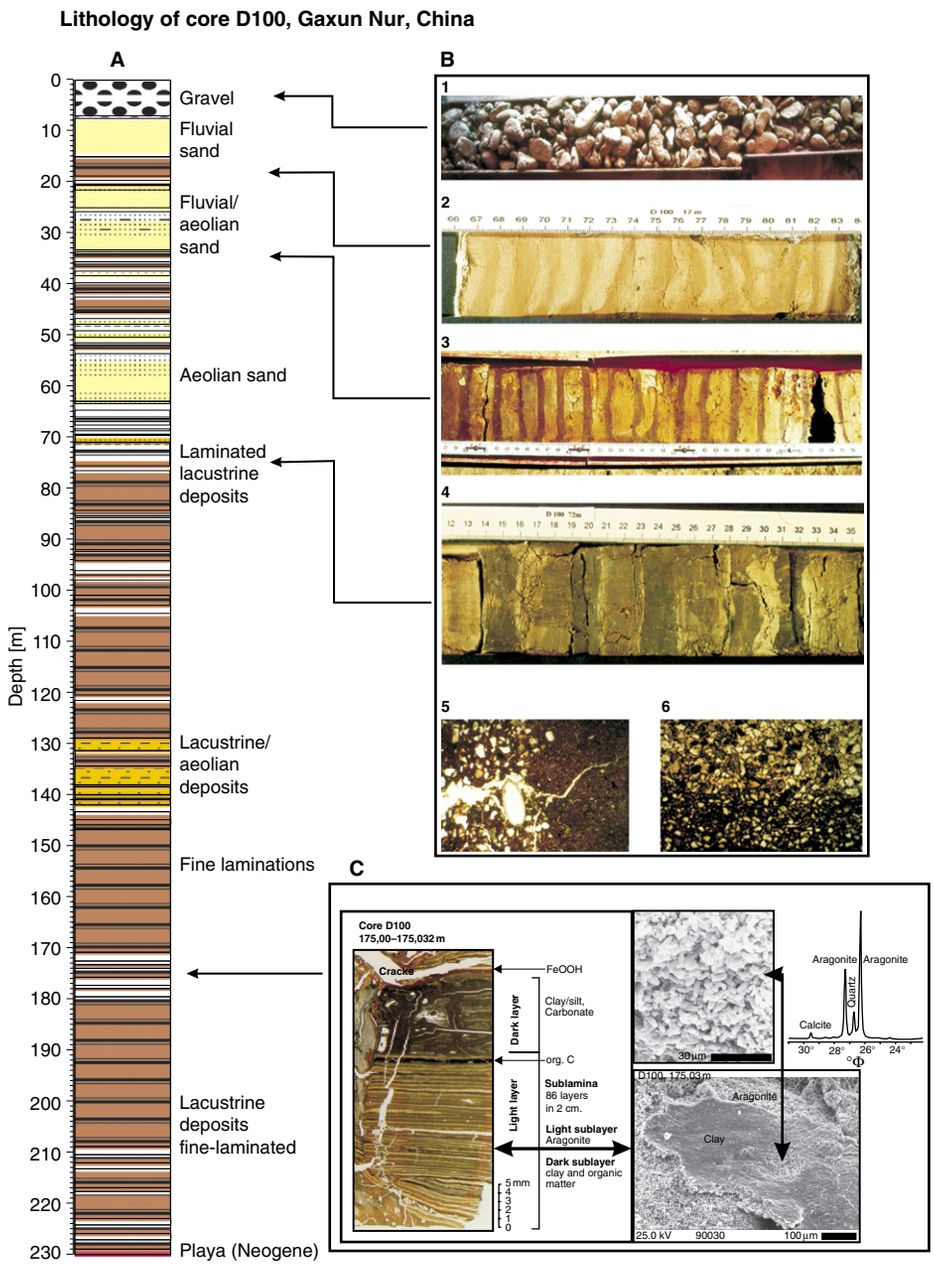

Fig. 22.4 Lithology of core 100, Gaxun Nur Basin. A = overview of the entire sediment core; B = photographs and thin sections of sediment sequences: ***1****: coarse gravel 0–7 m depth;* ***2****: laminated sand layers, 17.66–84 m depth;* ***3****: laminated silt-clay layers with dark layers <1 cm, 33.37–34.77 m depth;* ***4****: laminated silt-clay layers with dark layers 1–2 cm thick, 72.12–55 m depth;* ***5,6****: thin sections of laminated layers at 72 and 33.9 m depth. The dark layers contain more clay <1 µm in size, while only the light layers contain carbonatic fossil remains (here the brackish water tolerating ostracod Cyprideis torosa); C = Thin section, scanning electron microscope photos and XRD analyses of laminated sediments from 175 m depth. Sublaminations show variations between clastic input and authigenic aragonite precipitation.*

The coarse gravels of mainly metamorphic rocks (Figs. 22.4A, B1) up to 7 m depth indicate high-energy fluvial transport from local areas. They are widespread within the basin and cover lacustrine sediments. Stratified and E-W- or N-S-dipping layers are indicative of surface erosion along the northern (Gobi Altai Tienshan range) and western (Beishan Mts.) catchments of the basin. Sources from the Tibetan Plateau can be

excluded as the distance between the gravel plain and the Qilian Mts. is more than 350 km, too far away for coarse material to be transported into the interior of the basin. Poorly sorted, 2.5-m thick coarse-to-medium sands below the gravels complete the fluvial deposits and may indicate the initial phase of locally enhanced surface erosion. Limnic deposits beneath the fluvial components were AMS dated to 14 450 ± 100 yr BP, 15 060 ± 80, 17 390 ± 250 and 22 790 ± 150 yr (Table 22.1), indicating that the gravels and sands were formed after the LGM and probably during the Termination I and early Holocene.

Between 9.5 and 71.4 m depth, frequent alternations of well-sorted fine sand and silt layers occur (Fig. 22.4B2-6), indicating a playa-like depositional environment. For the first time, discontinuously laminated sequences of clay and silt occur between 16.24 and 20.58 m depth. They consist of dark (< 1 cm thick) and light layers (1–3 cm thick), with a mean grain size of 11 μm (Fig. 22.4B3-4). They are typical of a lacustrine facies which fills the main part of the Gaxun Nur Basin. Mineral composition and extremely high percentages of pelitic components indicate a long-distance transport as suspended load from the Tibetan Plateau via the Hei River. The dark layers differ from the light ones by significantly higher percentages of fine clay (< 1 micron, Fig. 22.4 B5-6) and lower carbonate content. We assume that these laminations do not represent annual deposition behaviour but more likely periods of flooding and depositional events, keeping a shallow lake inexistence for centuries or even millennia. Similar sequences occur at 51.97–52.22 m, 65.04–67.30 m and 68.24–70.15 m depth. They are interrupted either by aeolian sand (e.g. 21.55–25 m, 61.69–63.25 m and 70.15–71.46 m depth) or by semilacustrine sandy silt deposits. In some cases, alternations of sand and clayey silt (e.g. 50.18–52.60 m and 59.58–61.25 m depth) indicate that lacustrine sedimentation was probably overprinted by enhanced aeolian flux, thus leading to comparable event layers (Fig. 22.4B 2) as stated above.

From the general heterogeneity of the sediments down to 71.46 m depth, we assume that these different depositional processes require unstable hydrological conditions. Even complete desiccation of the playa system accompanied by stronger influence of aeolian processes might have occurred several times.

From 71.46 m downwards to 228.8 m depth, the sediments consist of silt and clay. Most parts are fairly well laminated (Fig. 22.4). They indicate that a perennial lake existed during the entire period of sedimentation, mainly supplied by freshwater from the Hei River. Coarser sediments (up to 250 μm) of aeolian origin only occur in single layers between 117 and 151 m depth, indicating additional input of dune sand from the vicinity of the lake.

Only selected sequences of the event layers have been counted so far. For example, 136 dark layers with a mean thickness of 1.8 cm appear between 73.7 and 78.6 m depth, indicating 27 flooding events per metre sediment. A similar value (26 events/m) accounts for 151.5–156.5 m depth, although the mean thickness of the dark layers is reduced to 1 cm, probably due to shorter durations of flooding events. On the other hand, variations in the thickness of light layers do not automatically indicate longer times of normal freshwater flux, rather, their thickness depends also on the amount of aeolian dust input (loess) from near-shoreline locations in phases of lake-level decline.

In several sequences below 165 m depth, sublaminations within light layers occur. Sub-millimetre thick dark layers of clay and organic matter alternate with authigenic aragonite, revealed by SEM and XRD analyses (Fig. 22.4C). Counting of sublamina from a thin section at 175 m depth revealed 43 single layers per centimetre pointing to annual varves of authigenically precipitated aragonite during summertime and deposition of clay during the cold seasons. Similar couplets were documented in

lake sediments from Lake Van, Turkey (Kempe and Degens, 1978).

Carbonatic fossil remains, classifying the sediments as lacustrine, have been found in several parts of the core, although they are not always present. Up to now, higher abundances of the ostracod shells *Limnocythere inopinata* and *Cyprideis torosa* as well as the freshwater gastropods assigned to the superfamilies Rissooidea and Cerithioidea (determined by S. Mischke and F. Riedel, Berlin) have been found in sequences at 68–74 m, 100–103 m, 119–125 and below 165 m depth.

22.5.2 Geochemical properties

For the interpretation of changes in the water balance of the Gaxun Nur Basin, we used the elements Ca, Mg and sulphur as the most appropriate ones to identify chemical precipitation of carbonates and sulphate in a lacustrine environment. They are indicative of increasing evaporation pressure over a water body and its residence time as well, both inducing rising salinity by the enrichment of ion concentration (Eugster and Hardie, 1978). SEM and XRD analyses of samples with higher concentrations of sulphur yielded evidence of gypsum formation when sulphur increased.

TOC is used to identify phases of increased internal productivity of the lake. The generally low values of TOC (0.2–1.6% dry weight, maximum 2%) in core D100 are quite normal for arid regions, where bioproductivity is limited owing to warm/cold and dry climate conditions. However, algae (e.g. Charophytes, *Pediastrum*) have been detected in various parts of the sediments and therefore indicate lake-internal bioprocesses which depend on water quality, temperature and depth. On the other hand, detrital input of organic matter (e.g. charcoal, wood remains and pollen grains) from the catchment of the lake was recognized too, leading to a certain enrichment of TOC in phases of intense river discharge. The total amount of residual silicates after loss on ignition is used to calculate the basic allochthonous sediment load transported either by the river from remote locations or by aeolian processes from the vicinity of the lake.

The geochemical properties in the sediments which can be used as climate proxies are summarized in Fig. 22.4, plotted against the depth of core D100 and divided into five units:

In unit 1 (160–144 m depth), relatively high values of up to 1.6% TOC are mainly derived from aquatic phytomass, developed during a period of positive water balance. Higher calcite (120–160 mg/g Ca) and gypsum ($\sim$4 mg/g sulphur) precipitation points to a slightly saline water body, interrupted by a distinct freshwater pulse (154–152 m depth). However, high calcite and moderate gypsum precipitation points to warm lake water as well as high phytomass production under mostly warm climate conditions. A reverse trend with more unfavourable conditions for lake-internal bioproductivity is detectable in the second half of unit 1.

Unit 2 (145–110 m depth) is characterized by generally low TOC ($<$0.5%), Ca ($<$40 mg/g), sulphur ($<$0.9 mg/g) concentrations and increased clastics, indicating a colder water body with reduced internal bioproductivity and external input of suspended load. Mg concentrations, indicative of Mg–calcite or even dolomite precipitation, remain constant, similar to unit 1. Two spikes of lowest Ca and sulphur at 143–141 m and at 135–132 m depth point to stronger changes in lake hydrology, resulting in a considerable lowering of the lake level, but without complete desiccation as suspended load appears to have been continuously accumulated. Close to the end of unit 2 (120–110 m depth) a return to more favourable conditions in terms of lake hydrology is detectable, with enhanced calcite, Mg–calcite and gypsum precipitation and reverse TOC contents. As Fig. 22.6 shows, we consider a general succession from freshwater inflow leading to rising lake levels, freshwater conditions and

increasing TOC followed by a steady state with increased residence time of the water and the enrichment of ion concentration towards saline conditions. The main chemical precipitate at that period is gypsum, pointing to a stepwise shrinkage of the water body under dry-warm conditions. Low amounts of detrital silicates at 110–113 m depth (Fig. 22.5) support the arguments of a reduced water inflow. Rising salinity may also have caused successive reduction of internal biological productivity as the low TOC values suggest.

Unit 3 (110–93 m depth) comprises a period of decreasing geochemical precipitates and TOC with minimum values of <20 mg/g Ca and $<0.4\%$ TOC at 106 and 102 m depth when clastic input is high. Grain-size analyses (see below) classify the clastics as predominantly aeolian silt and sand pointing to a generally negative water balance, similar to certain periods in unit 2. Surface inflow starts to increase again towards the end of unit 3.

Unit 4 (93–68 m depth) is characterized by frequent changes in TOC content between 0.4 and 2% as well as chemical precipitates (40–190 mg/g calcium, 6–40 mg/g magnesium and 6–20 mg/g sulphur) following the same succession as described above. These changes are due to short-term fluctuations in the water balance and evaporation intensity of generally unstable hydrological and climate conditions.

For unit 5 (68–11 m depth), only TOC and Ca data are available so far. Both datasets

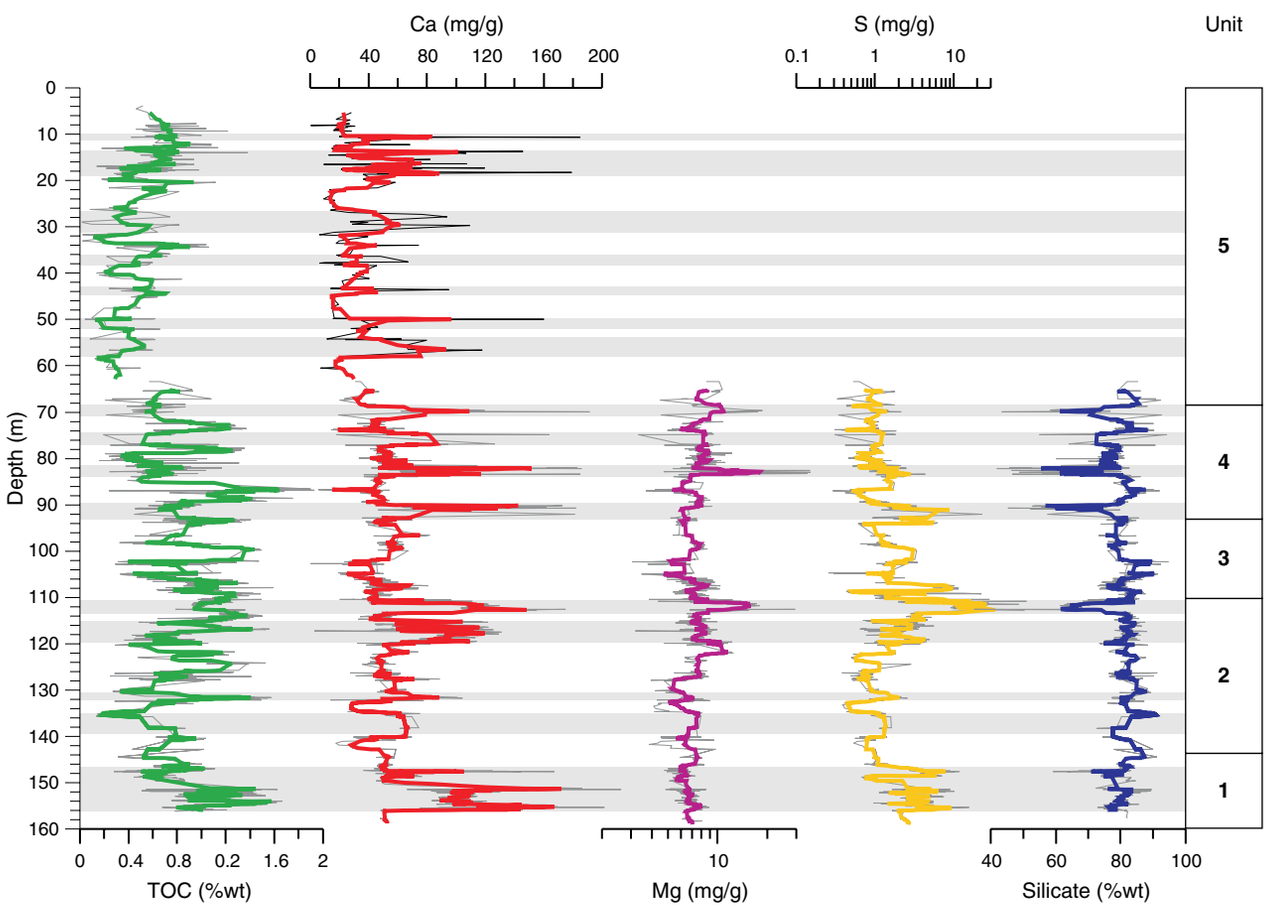

Fig. 22.5 Geochemical properties of the D100 core, Gaxun Nur Basin, NW China, between 7 and 160 m depth. The shaded areas in general mark periods of enhanced chemical precipitation and thus higher evaporation. Coloured graphs are 7-point low-pass filtered.

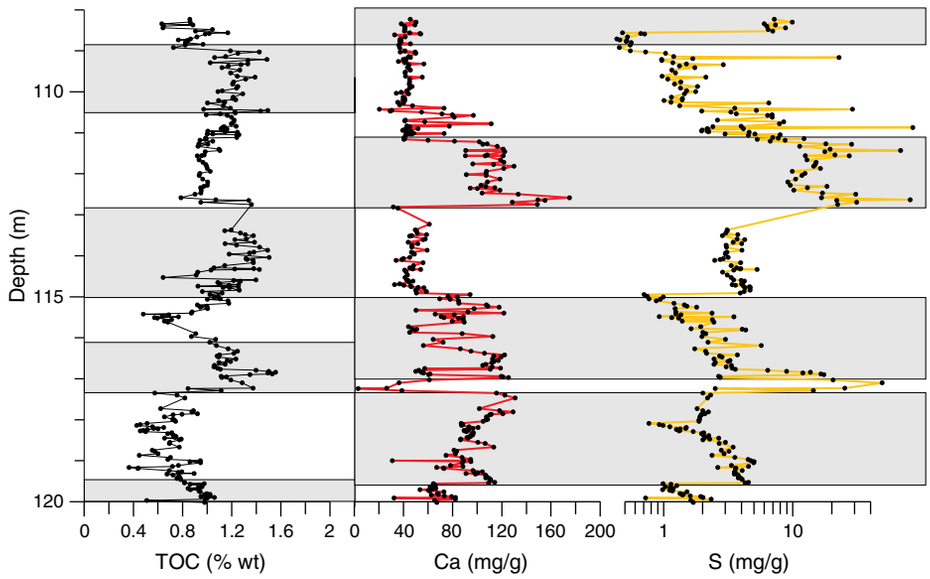

Fig. 22.6 TOC, Ca and sulphur (gypsum) distribution in core D100, 108–120 m depth. Changes in TOC content are inverse to carbonate or sulphate concentrations indicating organic development in phases of positive discharge under freshwater conditions while long residence time and shrinkage of the lake induce enhancement of ion concentration due to evaporation.

indicate similar fluctuations as in the previous unit but with generally lower values and amplitude. This is due to the fact that sediment in this unit changed more frequently between a lacustrine and semi-lacustrine facies to fluvial types, both superimposed by aeolian sedimentation under changing hydrological conditions. Phases of enhanced chemical precipitation at 58–50 m, 32–26 m and 20–11 m depth accord with stable lacustrine environments, while the lowest values fall in periods of enhanced dune sand accumulation at the drilling site, pointing to extremely low lake levels.

22.5.3 Grain-size variations

The classification in a triangular diagram (Fig. 22.7A) shows that the overwhelming majority of fine-grained sediments consists of silts. They are the main clastic components, either free of any sand fraction or with very small amounts of fine sand (63 – 200 µm). The clay fraction sometimes amounts to maximum 46% of the total volume. The median of samples is 11 µm, similar to the quartz median (Qmd) of the Luochuan loess section, reported by Xiao *et al.* (1995). The Gaxun Nur sediments cannot be characterized sufficiently by classical parameters such as mean, standard deviation, skewness and kurtosis, as many of the samples have bi- or even multimodal grain-size distributions. For example, the sample of Fig. 22.7B can be regarded as a typical unimodal clay-silt without any sandy component. The mode lies in the fine silt fraction, whereas the samples of Fig. 22.7C and 22.7D are typical multimodal silts with modes at 5 and 10 µm respectively, also containing variable proportions of coarse silt (modes at 25 and 53 µm) and fine sand (mode 160 µm). Especially in samples from dark layers (Fig. 22.7D), a further mode at 1 µm appears to be characteristic of higher clay components in those layers, probably accumulated after phases of flooding events. The enrichment of clay in dark layers may be due to coagulated clay particles which accumulated faster than noncoagulated ones.

The variation of grain-size distributions versus depth of D100 core is documented in Fig. 22.8. Assuming that different

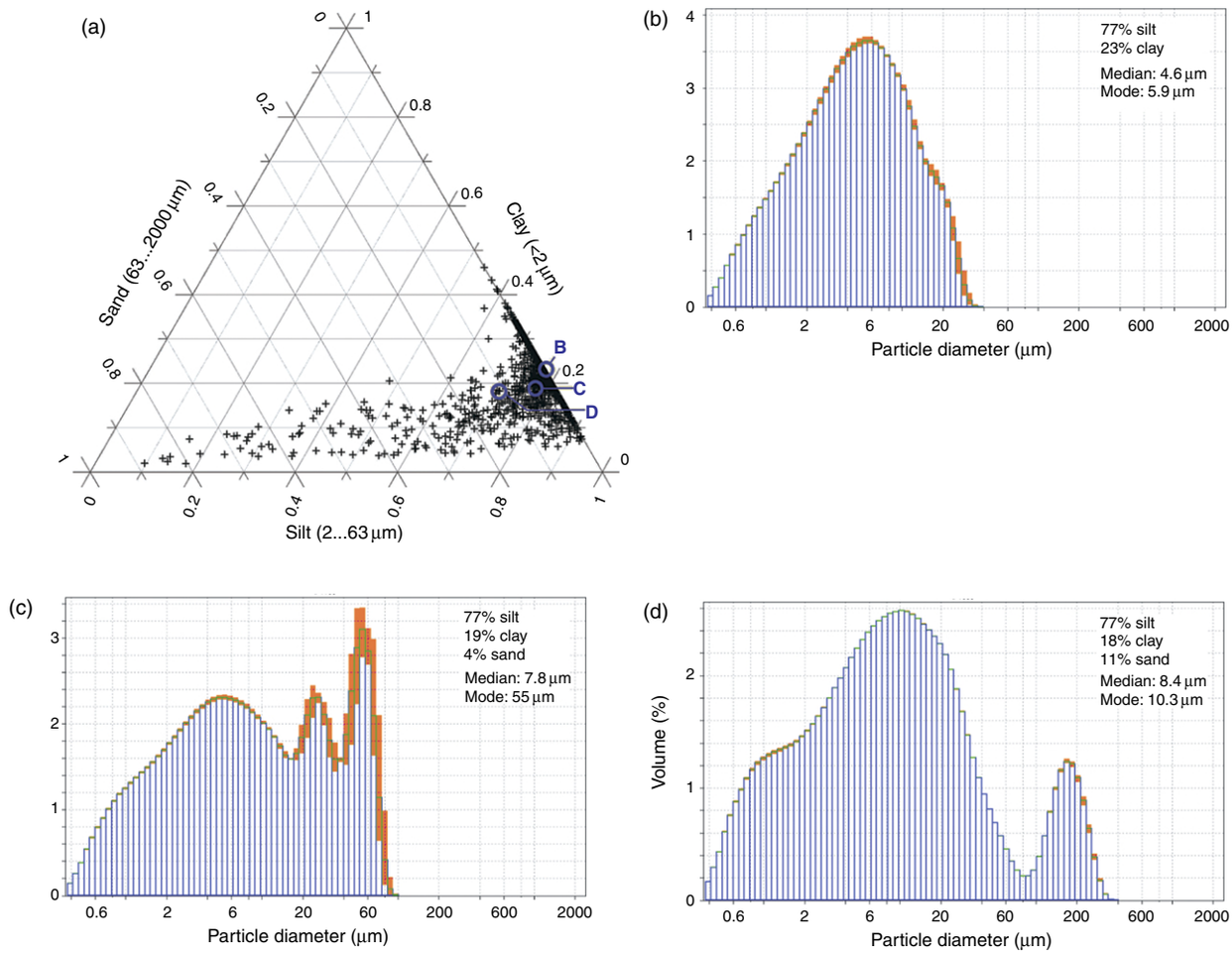

Fig. 22.7 Grain-size variations in sediments from the D100 core, Gaxun Nur Basin, NW China. a: Triangular diagram of all analysed samples. ***b, c****: Grain-size distributions of three clayey silts: b = unimodal silt, 77.34 m depth (light layer). c =* multimodal *silt, 115.62 m depth (dark layer). d: multimodal silt, 148.525 m depth (dark layer). Coloured areas mark deviations between single measurements.*

transport mechanisms are responsible for variations in grain size of clastic components that were deposited in a perennial but fluctuating lake, we can distinguish between two main depositional processes which contributed to the accumulation of the Gaxun Nur Basin: The fraction $<20\,\mu m$ was transported as suspended load (allochthonous clastics) into the basin mainly via the Hei River. As it was deposited into a stillwater body far away from the river mouth and from the lake shoreline, we assume that coarser clastics could not reach the drilling location during phases of high lake levels. On the other hand, we cannot exclude a certain amount of fine fractions deposited as aeolian dust within the lake. However, we assume that the majority of this grain-size fraction has been transported by fluvial processes. Its contribution of up to 80% of the whole sediment can be regarded as the basic load of clastic input. Even in sequences of coarse sand, up to 7% clay-silt is present.

The grain-size fractions $20-63\,\mu m$ and $63-200\,\mu m$ indicate aeolian transport of loess or dune sand from the vicinity of the lake to the drilling site. In contrast to the Luochuan loess section of the loess zone in China – where $44-16\,\mu m$ fractions were mainly deposited during cold periods whereas the smaller fractions ($16-5\,\mu m$) indicate deposition during interglacial climate conditions (Vandenberghe *et al.*, 1997) – our data cannot

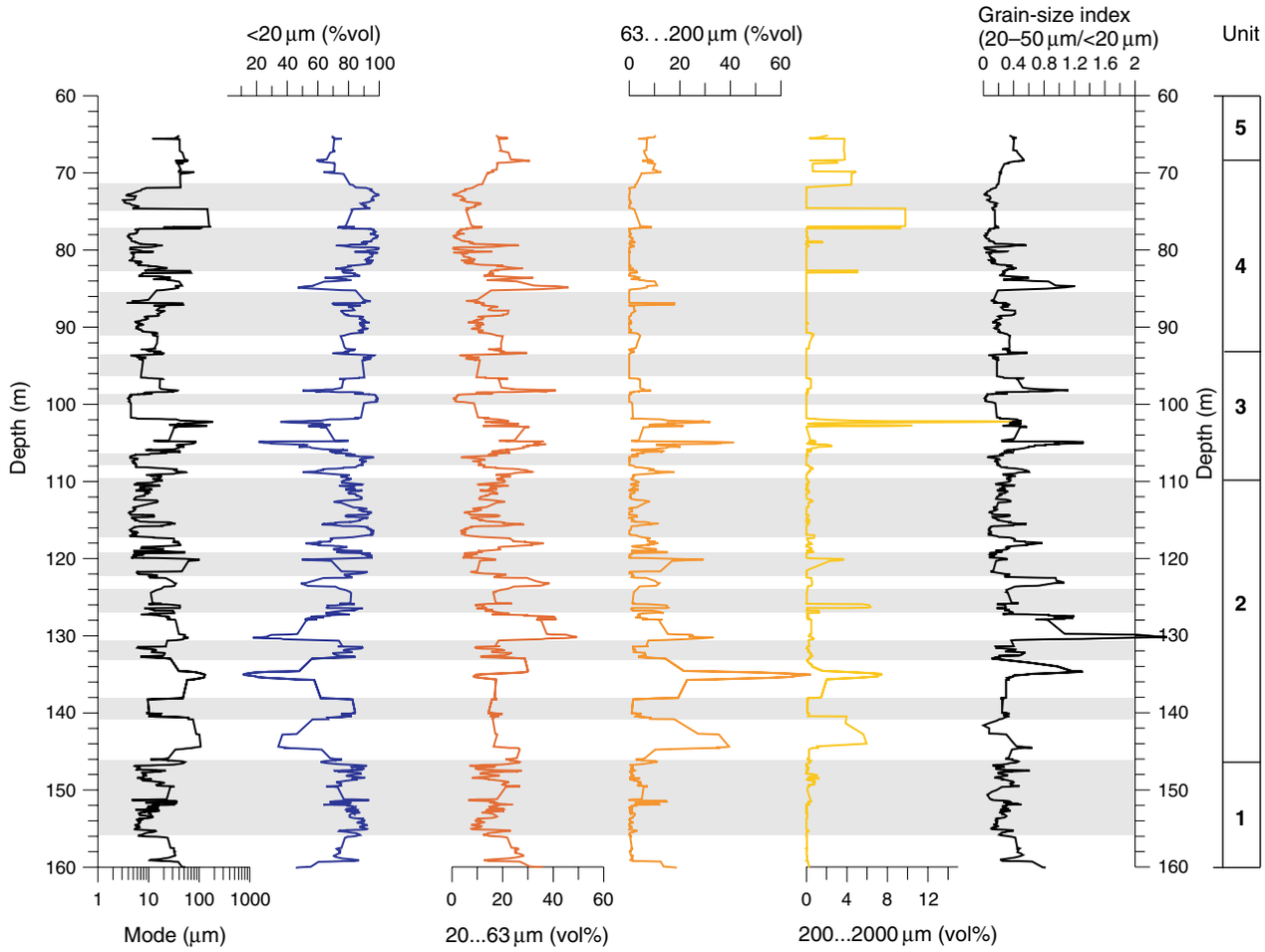

Fig. 22.8 Grain-size distribution (7-point low-pass filtered) in sediments of the D100 core, Gaxun Nur Basin, NW China, versus depth. Shaded areas mark phases of positive water balance, relatively high lake levels and reduced aeolian transport.

be used in the same way, as our site is located several hundred kilometres north-west of the Loess Plateau, a prominent source area of loess transport, where coarser fractions up to medium sand are the major aeolian components. However, the grain-size index used by Rousseau *et al.* (2002) for the Nussloch section in Germany may serve as an indicator of aeolian variability in the Gobi Desert too (see Fig. 22.8). Although it cannot be decided whether the coarser components are always transported by wind or sometimes probably reworked fluvial material, both processes at least require a shrinking lake, promoting the exposure of near-shore lake sediments which could be easily removed by the wind and transported to the centre of the lake and elsewhere.

Conversely, in phases of enhanced river discharge, expansion of the lake and higher lake levels, the distance between the lake shoreline and the drilling site increased considerably, reducing coarse clastic input (>70% of particles <20 µm, shaded parts in Fig. 22.8).

A relatively long period of stable/higher lake levels is also represented by sublaminated pelites (unit 1), only interrupted by short phases of aeolian input. At the transition from unit 1 to unit 2 and during the following unit 2 the input of aeolian components (loess and sandy loess) increases rapidly. In addition, medium and coarse sand (200–2000 µm grain size) of fluvial origin at 135 m depth indicates that the river mouth extended lake-ward

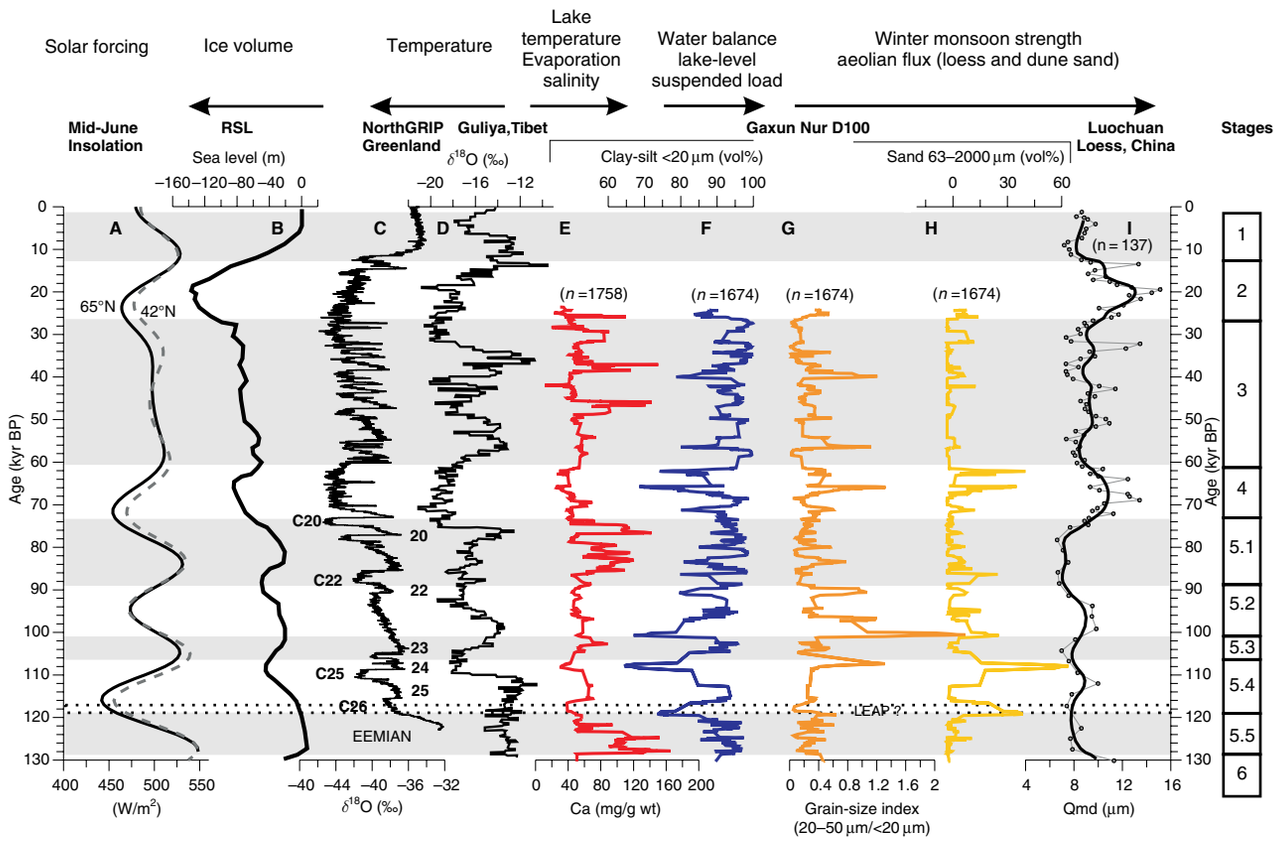

Fig. 22.9 Comparison of climate records with proxies from the D100 core, Gaxun Nur Basin, Gobi Desert, NW China. ***A****: Mid-June insolation for 65°N (solid line) and 42°N (dashed line) for the past 130 kyr.* ***B****: Relative sealevel (RSL) changes, adapted from Waelbroeck* et al. *(2002).* ***C****: NorthGRIP oxygen ice core record from central Greenland with selected numbers of cold stadials C26–C20 and interstadials (DO events), adapted from NorthGRIP Members (2004). D: Guliya ice core record from the central Tibetan Plateau, after Thompson* et al. *(1997).* ***E****: Calcium record from the D100 sediment core. E–H: Grain-size records (E =* suspended *load,* F = loess *component,* G = grain-*size index and* H = aeolian *sand) from the D100 sediment core. I: Quartz median record from the Luochuan loess section, adapted from Xiao* et al. *(1995). Data from the Gaxun Nur core D100 are 7-point low-pass filtered. Shaded areas mark warm-wet climate conditions, adapted from our data.*

due to a strong shrinkage of the lake which enabled coarse material to be deposited in the centre close to the drilling site. At the end of unit 2 (117–110 m depth), grain-size variations are similar to those in unit 1, indicating a more positive water balance and a more stable water body, although short-term fluctuations are detectable by high-frequency alternations between clay and silt. In unit 3 (110–93 m depth), the input of aeolian sand and coarser clastics of probably fluvial origin between 109 and 102 m is high again, implying an extremely negative water balance at that time. We assume that aeolian and probably fluvial inputs into a shrinking water body are the major processes at that time. Phases of higher suspended load indicating more stable lake conditions and thus higher lake levels throughout unit 3 and the following unit 4 appear at 96–94 m, 91–85 m, 83–77 m and 74.5–70.5 m depth. However, they are always interrupted by short-term phases of enhanced aeolian input into an existing lake. The change from predominantly fine-grained lacustrine deposits to sandy silt and finally dune sand from

71.4 m depth upwards supports the arguments of a generally deteriorating water balance in the Gaxun Nur Basin.

22.6 DISCUSSION

Lithology, geochemical properties and grain-size distributions of the D100 core from the Gaxun Nur Basin provide evidence for repeated changes in the water balance of an extended palaeolake within the Gobi Desert of north-western arid China. Our chronology indicates that the sediment records from the D100 core comprise the history of the past 250 kyr. However, we focus on the results of the upper 160 m of the core, i.e. the last 130 kyr (Fig. 22.9), thus covering the period from the last interglacial to the early part of the LGM ($\sim$25 kyr). We compare our records with ice core data from Greenland (NorthGRIP Project Members, 2004) and Tibet (Thompson *et al.*, 1997), with the relative sea-level record (Waelbroeck *et al.*, 2002) and with the Luochuan loess record from the Chinese Loess Plateau as well (Xiao *et al.*, 1995; Rousseau and Wu, 1997).

Considering that the geochemical proxies (salinity and evaporation–precipitation ratio) and grain-size parameters (suspended load and aeolian transport) have a direct relation to changes in hygric conditions of the Gaxun Nur Basin and its catchment, we can set up following presumptions: Increased suspended load requires a substantial increase of river discharge towards the basin, triggered either by enhanced precipitation in the catchment and/or by melt water discharge, both resulting in the growth of lake size and water volume. As our drilling site in the centre of the basin is located far distant from the river mouth/shorelines, we assume that coarser sediment fractions were deposited by aeolian input as (sandy) loess. Fluvial input was only possible when the distance between the coring site and the river mouth/shorelines decreased considerably. The latter requires a strong shrinkage of the lake in phases of reduced surface discharge. Furthermore, considering a substantial contribution of melt water towards the basin during the last glacial cycle, we also assume that melt water flux rose when snowmelt in the upper catchments was high due to increased temperatures and vice versa. This would mean that changing annual mean temperatures in the upper catchments (above and below the snowline), generally detectable by the oxygen-18 proxies from ice cores (Thompson *et al.*, 1989, 1997; Thompson 2000), must have had an influence on the dynamics of the glaciers themselves, leading to either glacier advance in phases of colder and/or wetter conditions or glacier decay in periods of warming and/or decreasing precipitation. Hence, we hypothesize that glacier advance in Tibet requires a temporal shift of effective moisture supply from summer to autumn and wintertime to keep the glaciers growing. Such shift would also lead to a drop in the annual temperature, which is isotopically preserved in glaciers. Consequently, stable oxygen isotope signatures in glacier ice of Tibetan glaciers not only indicate temperature changes but also imply dynamic processes towards glacier growth or decay.

22.6.1 The last interglacial (MIS 5, 129–72 kyr BP)

The warm stage of the last interglacial (MIS 5.5) appears in our records as a period of enhanced water discharge from southern regions (Tibetan Plateau) towards the basin which led to a rapid development of a large lake, coeval with a reduction of aeolian flux (Fig. 22.9G–I). According to our data, the transition from MIS 6 to MIS 5.5 is defined in the grain-size records by a simultaneous drop in aeolian activity and a rise in surface discharge at about 129 kyr, equal to 156 m core depth. Lowest sulphur and calcium values indicate a still reduced evaporation pressure and low water temperatures at that time. A rapid warming during the following

1000 years is indicated by sudden increases in water temperature, residence time and evaporation, with rising salinities peaking at about 128 kyr. This phase of warmer and moister climate conditions comprises the time from the inception at 129 kyr to about 119 kyr, inferred from our age model (see Section 4). High calcite precipitation and surface discharge of nearly 10 000-year duration (Fig. 22.9E, F) indicate a stable aquatic environment, while a long residence time of the water body and strong evaporation may have caused increasing salinity under at least warm moist climate conditions. The intermittent distinct freshwater pulses in the middle part of this warm stage led to several refillings of the lake without a general change in climate conditions. Hence, it seems plausible to assume that these refillings towards freshwater conditions were due to enhanced rainfall in the catchment of the lake triggered by a strengthened SE summer monsoon.

The lack of aeolian sand and a low grain-size index (Fig. 22.9G, H) in our record during that period support the assumption of reduced aeolian transport because most of the potential source area was covered by water and vegetation. This period of reduced dust flux and the development of a large lake within the Gaxun Nur Basin coincides with the formation of the S1 soil on the Loess Plateau (e.g. Kukla and An, 1989; An *et al.*, 1991; An and Porter, 1997) and with lake formation in the Zoige Basin, north-eastern Tibetan Plateau (Chen *et al.*, 1995). They all require warm-moist climate conditions in both high and low altitudes during substage 5.5, similar to the present climate or even warmer (Frenzel, 1994). Accordingly, the Guliya ice core record from central Tibet (Fig. 22.9D; Thompson *et al.*, 1997) shows less negative oxygen-18 values, indicating higher temperatures over the Tibetan Plateau. Hence, we assume increased temperatures at high altitudes which may have caused high melt water flux during the summer season, resulting in negative glacier balances in the upper catchments of the Gaxun Nur system. This is supported by the fact that the sea level of the South China Sea was equal to the present coastline (Yang, 1991) or even slightly higher (Jouzel *et al.*, 2002; Waelbroeck *et al.*, 2002; Shackleton *et al.*, 2003). Both melt water and more frequent summer monsoon rainfall may have promoted the strong surface discharge towards the basins. Maher and Thompson (1995) calculated mean precipitation values on the basis of magnetic susceptibility data from loess sections and assume that rainfall north of the Qinghai-Tibetan Plateau during the last interglacial was two to three times higher than at present. Consequently, the summer monsoon front must have shifted some hundred kilometres northwards to back up sufficient rainfall in the presently dry desert, also assumed by An (2000). However, we are not able to quantitatively calculate the mean annual precipitation in the Gaxun Nur Basin during warm stage 5.5, but the existence of a large and biologically active water body supports our assumption of warm and moist climate conditions with potentially longer summer monsoon impact and shorter cold-dry winter seasons.

According to our chronology, favourable climate conditions and a high lake level (but with a general decreasing trend) existed until 119 kyr. Small grain-size diameters (Fig. 22.9I) indicate a generally weak winter monsoon at that time. The most stable fresh-to-slightly brackish water conditions of about 7000-year duration occurred between 128 and 121 kyr, followed by a rapid desiccation and increase in dust flux (Fig. 22.9E–H) which culminated at about 119 kyr, equal to 144.7 m core depth. Owing to low data resolution, this environmental trend is not preserved in the Luochuan loess section. However, a comparison with the NorthGRIP ice core record (Fig. 22.9C) indicates that the change in lake hydrology towards a negative water balance corresponds to the rapid depletion of the oxygen-18 isotopes at the end of stage 5.5. We therefore assume a shift towards colder

and drier climate conditions, also associated with a global sea-level drop of about 20 m at ca. 118 kyr BP (Fig. 22.9B) at least. As the severe drop in river discharge is accompanied by low carbonate precipitation and suspended load as well as high input of dune sand, we interpret this abrupt change as a signal for colder and drier climate conditions which may have prevailed for about 500–800 years. This short climate spell may correspond to the 468-year long late Eemian aridity pulse (LEAP), reported from central Europe by Sirocko *et al.* (2005) and terminates the warm-wet substage 5.5 in north-western China.

With respect to the timing and duration of this substage, our data imply that the warm-wet climate phase between 129 and 119 kyr comprises the Eemian in north-western China. Compared with vegetation and marine records from western Europe, where the Eemian (MIS 5e) is considered to cover the period from 126 to 110 kyr (Shackleton *et al.*, 2003; Sánchez Goñi *et al.*, 1999, 2005), our time range for the Eemian is, however, strikingly different. In our opinion, this mismatch is primarily due to the fact that the desert regions in an extreme continental position north of the Tibetan Plateau responded immediately and very sensitively to changes in moisture availability, rather than to changes in local temperature. As the Gaxun Nur Basin is directly connected with glaciated high mountain ranges, both major changes in glacier budgets and alternations in moisture transporting air masses promptly affect the hydrological system in the Tibetan foreland, promoting either lake formation or aeolian activity. By contrast, vegetational changes (especially in trees) follow with a certain time lag, when plant-available water and the groundwater table have been stabilized and vice versa. However, we cannot decide whether the time lags of 3000 years for the onset and even 9000 years for the end of the Eemian can be explained by these relations alone. As the duration of the Eemian in northern Europe (126–115 kyr; Sánchez Goñi *et al.*, 2005) is much closer to our chronology, we assume that regional disparities of the Eemian not only depend on latitudinal climate differences but probably also on continentality. Palynological records from north-western China which could prove this assumption are still lacking.

In terms of water availability, our data imply that during the succeeding substages of MIS 5 alternations from positive to negative balances do not differ strikingly from those during the warm-wet stage 5.5. However, the amplitudes between high and low river discharges increase considerably, likewise the amount of aeolian transport. Both indicate more frequent and intense changes between the extremes than before. Hence, we assume that the onset of glacier growth since the last glacial inception at about 118 kyr, most likely triggered by decreased insolation (Fig. 22.9A; Berger and Loutre, 2002; Calov *et al.*, 2005), is the major reason for instable climate conditions in the catchment of the Gaxun Nur Basin since the termination of the Eemian.

In phases of high river discharge and reduced aeolian transport (Fig. 22.9G-I), roughly correspondent with the D/O events 25–20 in the NorthGRIP ice core record (Fig. 22.9C), increased melt water flux and monsoon precipitation may have dominated to keep the water balance of the Gaxun Nur positive. According to our data, this happened during the first half of substage 5.4 (ca. 117–111 kyr) and during the substages 5.3 (106–101 kyr) and 5.1 (89–74 kyr). Small grain-size diameters in the Luochuan loess section (Fig. 22.9I) supplement our assumption of repeated millennial scale warm-moist climate pulses with high lake levels. The mollusc record from the Luochuan loess section even indicates that at about 88 kyr the climate on the Chinese Loess Plateau was warmer and wetter than today (Rousseau and Wu, 1997), but increasing chemical precipitates with enhanced gypsum formation afterwards point to a general trend towards aridification. According to Dansgaard *et al.* (1993), these phases of enhanced evaporation may correspond to

DO events 23 (Brørup-Interstadial) and 21 (Odderade-Interstadial). Intermittent freshwater pulses from the south kept the lake in existence (see also Fig. 22.6).

However, the climate might have been considerably different from the warm-wet Eemian substage which was characterized by locally enhanced summer monsoon rainfall buffering phases of reduced river discharge at that time. By contrast, lake phases between 118 and 74 kyr were mainly controlled by the run-off from the Tibetan catchments with increased rainfall and melt water flux there. Additional but limited water supply may have only resulted from local rainfall during the warm seasons, generated by a convective water vapour circle over a large water body, as previously assumed by Pachur *et al.* (1995). Summer monsoon rainfall in that region can be excluded, as the continuously increased albedo over the Tibetan Plateau has inhibited a considerable northward shift of the summer monsoon front.

High-frequency alternations in the water balance of the Gaxun Nur Basin during the substages 5.3–5.1 also indicate that millennial scale periods of enhanced freshwater input are the major reasons for the deposition of laminated lacustrine sediments < 20 mm in size (Fig. 22.9F) into a perennial and probably deep lake. The laminated dark and light layers indicate periodical flooding events, which most likely occurred cyclically two to three times per century. The majority of such freshwater pulses are especially pronounced during the interstadial substages 5.3 and 5.1.

Lowest discharge rates and enhanced aeolian flux within the Gaxun Nur Basin culminate during the substages 5.4 (second half, 108–106 kyr) and 5.2 (around 100 and 92–90 kyr), not exactly in phase with the Greenland and Tibetan ice core records. However, fluvial sand and high loess contents in the D100 core reflect lowest lake levels and vast areas of exposed lake sediments now easily deflated and transported southwards to the Chinese Loess Plateau, owing to a strengthened winter monsoon (Xiao *et al.*, 1995; Porter and An, 1995). In particular, coarser grains in the Luochuan loess section (Fig. 22.9I) indicate the coherence of exposed lacustrine sediments during phases of negative water balance and their transport to the loess regions of China by enhanced wind activity.

22.6.2 The cold stage 4 (74–60 kyr)

The most severe cold phase during the last glacial cycle is well recorded in both Greenland and Tibetan ice cores (Fig. 22.9C, D). Cold and even dry conditions between 74 and 60 kyr are also detectable in the Gaxun Nur record by strong increases in aeolian flux, peaking at 72, 67 and 62 kyr, generally in agreement with the main occurrence of xerophilous mollusc taxa in the Luochuan loess section between 75 and 60 kyr, reflecting drier conditions than today (Rousseau and Wu, 1997). In contrast to the ice core and loess records, our data indicate an intermediate wet spell with enhanced river discharge between 70 and 68 kyr (Fig. 22.9, F–H), also identifiable in the Luochuan mollusc record (Rousseau and Wu, 1997, Fig. 22.3), which seems to have interrupted the cold-dry conditions north and east of the Tibetan Plateau for a 2000-year long period. One possible explanation for this mismatch with the ice core records might be the fact that parallel to the massive glacier advance in Tibet melt water flux towards the dry foreland increased dramatically and refilled the terminal lake. The coherence of glacier advance and high melt water flux in the catchment of the Gaxun Nur is only possible if we consider effective moisture supply at that time, not by the summer monsoon but more likely by the westerlies during late summer/early autumn. Snowfall in high altitudes then became most effective due to decreased summer radiation, while in lower altitudes (below the snowline) local precipitation and continuing ice melt contributed to increased surface run-off. This would also explain why enhanced wind

velocities and dust transport from western directions resulted in loess accumulation on the Loess Plateau (Vandenberghe *et al.* 1997), while dust flux in the Gaxun Nur area remained low.

From about 68 kyr onwards, the dramatic shrinkage of the Gaxun Nur lake promoted the exposure of fine-grained lacustrine deposits leading to deflation by wind erosion, transportation to south-eastern locations and deposition there as loess. This pathway of loess transport requires a stronger influence of the winter monsoon under cold-dry climate conditions which prevailed until about 60 kyr. Increased particle size in loess sections of the Loess Plateau (Fig. 22.9I, An *et al.*, 1991; Porter and An 1995) confirms the intensive wind activity at that time.

22.6.3 The interstadial stage 3 (60–24 kyr)

The climate conditions during MIS 3 are marked by strong alternations of warm-wet and cold-dry pulses within the Gaxun Nur catchment, corresponding to fluctuations in the global sealevel (Fig. 22.9B). In terms of water budget, the temporal variations in the Gaxun Nur Basin reflect a close relationship to temperature-dependent isotopic changes of the NorthGRIP and Guliya ice cores, although not all cycles recorded there resulted in synchronous responses within the drylands of north-western China. However, phases of positive water balance with highest lake levels also in adjacent areas fall in periods of relatively warm and moist climate conditions (Pachur *et al.*, 1995; Wünnemann *et al.*, 1998; Zhang *et al.*, 2001, 2002) with enhanced Indian monsoon (Shi *et al.*, 2001), when melt water discharge was effective owing to the melting of the Tibetan glaciers. Similar to the climate conditions during the substages 5.4–5.1, the water balance of the Gaxun Nur system during stage 3 was mainly controlled by surface discharge from the Tibetan Plateau.

Evidence for enhanced local precipitation within the Gaxun Nur Basin at that time is lacking so far. However, some information about the vegetation history (Ma *et al.*, 2003) points to poorly developed desert grassland and gallery forests along the rivers, although the freshwater lake expanded to $>10\,000\,km^2$ at about 30 kyr ago (Wünnemann, 1999; Hartmann, 2003). Prior to this event, phases of reduced lake levels at 57–55, 50–48 and 42–40 kyr coincide with enhanced loess transport (Fig. 22.9 F, G) and ice rafted debris (IRD) in the North Atlantic (McManus *et al.*, 1999) On the other hand, mobile dune sand could not reach the centre of the lake, because the lake size remained large enough for sand to be transported by wind from the lake shore to the centre. Climate conditions were favourable for sand transport into the basin only just after phases of enhanced chemical precipitation of carbonates and sulphates (Fig. 22.8D), indicating a stepwise shrinkage of the lake after 47, 38, 32 and 26 kyr. Periods of warmer climate conditions and higher amounts of chemical precipitates roughly match interstadial phases of glacier decay in Tibet, whereas low lake levels and high loess transport generally match stadials of enhanced glacier advance and colder climate. As peaks of coarser loess in the Luochuan section (Fig. 22.9I) appear during phases of high lake levels in the Gaxun Nur Basin when most of the deflatable sediments were covered by water, we assume that loess transport at that time was probably more strongly affected by the westerlies, similar to the wind regime during the transitional phase from substage 5.1 to 4.

22.6.4 The LGM within stage 2 (LGM, 24–21 kyr BP)

After the transition from stage 3 to the LGM at about 25 kyr, the aeolian influence increased remarkably, as inferred from aeolian deposits between 63 and 54 m core depth (Fig. 22.4A), while the water balance of the Gaxun Nur basin became as negative

as in previous cold stages without complete desiccation. Increased aeolian flux since about 25 kyr coincides with the increase of coarse quartz grains in loess sections (Fig. 22.9I, Porter and An, 1995), both indicating increased wind strength under cold-dry climate conditions, leading to a strong expansion of the desert belt of about 20° longitude (Sun *et al.*, 1998). Our proxy record ends at the transition from lacustrine to semilacustrine and fluvially dominated sediments after 24 kyr. However, previous investigations (Wünnemann, 1999) show a continuation and even increase of the aeolian component under very shallow water conditions throughout stage 2. Fluvially transported sand and suspended load from northern and western catchments of the basin since the termination of stage 2 indicate a successive refilling of the lake as a result of locally enhanced rainfall by a strengthened summer monsoon after 14 kyr (Wünnemann and Hartmann, 2002).

Kohfeld and Harrison (2003) calculated that during stage 2 wind strength and mass accumulation rates were roughly 4.3 times higher than during stage 5. By contrast, our data indicate that wind intensity and aeolian flux during the cold substages of stage 5 and during stages 4 and 2 were probably not extremely different. Comparison with the Luochuan loess section supports our assumption of repeated dust fluxes with similar magnitudes during stages 4 and 2 and lower magnitudes during stages 5 and 3. More important is the fact that the duration of dust transport and the flow direction of loess-transporting air masses may have changed considerably through time. They probably had much stronger impact on depositional conditions than known so far. Further research on this topic is required.

22.6.5 Conclusion

Our record from the Gaxun Nur Basin displays severe changes in the water balance during the last glacial cycle. On the assumption that our chronology is correct, phases of positive water balance and thus the expansion of the terminal lake within a flat desert environment quite precisely follow global and regional patterns of highly variable climate conditions during the last interglacial and glacial cycle as documented in ice cores from Greenland and Tibet.

During the warm interglacial stage 5.5, equal to the Eemian, the water balance of the Gaxun Nur system was controlled both by surface discharge from the northern and southern catchments of the lake and by sufficient local rainfall. It seems most likely that the necessary moisture supply was due to an intensified SE summer monsoon. This period of warm-wet climate conditions in Central Asian deserts during the last interglacial also prevailed in the Sahara as reported by Yan and Petit-Maire (1994) and Thiedig *et al.* (2000), indicating a marked decrease in desert environments along the Old World dryland belt. However, detailed palaeoclimate records which could prove the interglacial climates in the desert regions of China are still lacking. Conversely, periods of positive water balance in the Gaxun Nur Basin during the following cycles were mainly controlled by the surface discharge from the glaciated Tibetan Plateau. Glacier melt water and local rainfall in the upper catchment of the Hei River were the main sources of water supply towards the basin. Glacier advance in northern Tibet and enhanced rainfall in lower altitudes during phases of climate cooling may have been triggered by the influence of the westerly waves which provided the necessary moisture in late summer and early autumn to keep the glaciers growing. Consequently, the seasonal southward shift of the summer monsoon probably started earlier, while the Siberian high-pressure cell was not fully developed. This scenario would enable moist air masses to flow from western regions eastwards more frequently and use pathways along the west–east striking mountain barriers of the Tibetan Plateau.

The periodically repeated climate changes in arid China are closely connected to global climate signatures mainly driven by solar

forcing. Major climate changes throughout the last 130 kyr follow the insolation anomalies on a precessional band (Fig. 22.9A). However, our record shows that short-term variations of freshwater and aeolian fluxes respond to the East Asian Monsoon evolution (An *et al.*, 1991; Porter and An 1995; An, 2000) and to the westerlies system as well (Pachur *et al.*, 1995; Vandenberghe *et al.*, 1997), both driven by a nonlinear pattern of thermohaline circulation and changes in ice volume (e.g. Ding *et al.*, 1994).

The synchronized coherence of loess transport from the Gaxun Nur Basin towards the Loess Plateau (Luochuan section) during cold events, comparable to those preserved in the Greenland ice cores and to IRD events (e.g. Xiao *et al.*, 1995; McManus *et al.*, 1999) indicates that cold dry air masses in the North Atlantic region may have fundamentally interacted with the winter monsoon and the westerlies over China.

ACKNOWLEDGEMENT

This research was funded by the German Ministry of Science and Technology (BMBF), grant UF-UFLD01097800-01LD0041 and by the Deutsche Forschungsgemeinschaft (DFG, Pa 161/16-4). We thank D. D. Rousseau, M. L. Siggaard-Andersen and M. F. Sánchez Goñi for their critical comments and suggestions to improve our manuscript.

REFERENCES

An, Z., 2000. The history and variability of the East Asian paleomonsoon climate. Quaternary Science Reviews 19, 171–187.

An, Z.S., Porter, S.C., 1997. Millennial-scale climatic oscillations during the last interglaciation in central China. Geology 25, 603–606.

An, Z.S., Kukla, G.J., Porter, S.C., Xiao, J., 1991. Magnetic susceptibility evidence of monsoon variation on the Loess Plateau of Central China during the last 130 000 years. Quaternary Research 36, 29–36.

An, Z., Kutzbach, J.E., Prell, W., Porter, S.C., 2001. Evolution of Asian monsoons and phased uplift of the Himalaya–Tibetan plateau since Late Miocene times. Nature 411, 62–66.

Becken, M., Hölz, S., Polag, D., Fiedler-Volmer, R., Burkhardt, H., 2003. Electromagnetic investigation in the Gaxun Nur Basin, Inner Mongolia, China. In: Mischke, S., Wünnemann, B., Riedel, F. (Eds), International Symposium-Environmental Change in Central Asia. Department of Earth Sciences, Berlin, Abstracts, 8–10.

Berger, A., Loutre, M.F., 1991. Insolation values for the climate of the last 10 million years. Quaternary Science Reviews, 10, 297–373.

Berger, A., Loutre, M.F., 2002. An exceptionally long interglacial ahead? Science 297, 1287–1288.

Bond, G., Showers, W., Cheseby, M., Lotti, R., Almasi, P., deMenocal, P., Priore, P., Cullen, H., Hajdas, I., Bonani, G., 1997. A pervasive millennial-scale cycle in North Atlantic Holocene and glacial climates. Science 278, 1257–1266.

Calov, R., Ganopolski, A., Claussen, M., Petukhov, V., Greve, R., 2005. Transient simulation of the last glacial inception. Part I: Glacial inception as a bifurcation in the climate system. Climate Dynamics 24, doi: 10.1007/s00382-005-0007-6.

Chen, F., Wang, S., Li, J., Shi, Y., Cao, J., Zhang, Y., Wang, Y., Kelts, K., 1995. Paleomagnetic record from RH lacustrine core in Zoige Basin of the Tibetan Plateau. Science in China, Ser. B 38 (12), 1513–1521.

Clement, A.C., Cane, M.A., Saeger, R., 2001. An orbitally driven tropical source for abrupt climate change. Journal of Climate 14, 2369–2375.

Cunningham, W.D., Windley, B.F., Dorjnamjaa, D., Badamgarov, J., Saandar, M., 1996. Late Cenozoic transpression in southwestern Mongolia and the Gobi Altai-Tien Shan connection. Earth and Planetary Science Letters 140, 67–81.

Dansgaard, W., Johnsen, S.J., Clausen, H.B., Dahl-Jensen, D., Gundestrup, N.S., Hammer, C.U., Hvidberg, C.S., Steffensen, J.P., Dveinbjörnsdottir, A.E., Jouzel, J., Bond, G., 1993. Evidence for general instability of past climate from a 250-kyr ice-core record. Nature 364, 218–220.

Ding, Z.L., Yu, Z.W., Rutter, N.W., Liu, T.S., 1994. Towards an orbital time scale for Chinese loess deposits. Quaternary Science Reviews 13, 39–70.

Domrös, M., Peng, G., 1988. The Climate of China. Springer, Berlin, 350 pp.

EPICA Members, 2004. Eight glacial cycles from an Antarctic ice core. Nature 429, 623–628.

Eugster, H.P., Hardie, L.A., 1978. Saline lakes. In: Lerman, A.B., (Ed.), Lakes-Chemistry, Geology, Physics, Springer, 237–293.

Frenzel, B., 1994. Zur Paläoklimatologie der letzten Eiszeit auf dem Tibetischen Plateau. Göttinger Geographische Abhandlungen 95, 115–141.

Gansu Provincial Geological Bureau, 1980. Geological report on 1:200 000 scale geological survey (in Chinese), Lanzhou Press.

Hartmann, K., 2003. Spätpleistozäne und holozäne Morphodynamik im nördlichen Gaxun Nur Becken, Innere Mongolei, NW- China. Dissertation FU Berlin, 1–123.

Hetzel, R., Niedermann, S., Tao, M., Kubik, P.W., Ivyochs, S., Strecker, M.R., 2002. Low slip rates and long-term preservation of geomorphic features in Central Asia. Nature 417, 428–432.

Jouzel, J., Hoffmann, G., Parrenin, F., Waelbroeck, C., 2002. Atmospheric oxygen 18 and sealevel change. Quaternary Science Reviews 21, 307–314.

Kempe, S., Degens, E.T., 1978. Hydrographie, Warvenchronologie und organische Geochemie des Van-Sees, Ost-Türkei. In: Degens, E.T., Kurtmann, F. (Eds), The Geology of Lake Van, Ankara, 56–63.

Kohfeld, K.E., Harrison, S.P., 2003. Glacial–interglacial changes in dust deposition on the Chinese Loess Plateau. Quaternary Science Reviews 22, 1859–1878.

Kukla, G., An, Z., 1989. Loess stratigraphy in Central China. Palaeogeography, Palaeoclimatology, Palaeoecology 72, 811–814.

Leuschner, D.C., Sirocko, F., 2003. Orbital insolation forcing of the Indian Monsoon – a motor for global climate changes? Palaeogeography, Palaeoclimatology, Palaeoecology 197, 83–95.

Li, Y., Yang, J., Tan, L., Duan, F., 1999. Impact of tectonics on alluvial landforms in the Hexi Corridor, NW China. Geomorphology 28, 299–308.

Ma, Y.Z., Zhang, H., Pachur, H.-J., Wünnemann, B., Li, J., Feng, Z., 2003. Late Glacial and Holocene vegetation history and paleoclimate of the Tengger Desert, northwestern China. Chinese Science Bulletin 48, 1457–1463.

Maher, B.A., Thompson, R., 1995. Paleorainfall reconstructions from pedogenic magnetic susceptibility variations in the Chinese loess and paleosols. Quaternary Research 44, 383–391.

McManus, J.F., Oppo, D.W., Cullen, J.L., 1999. A 0.5-million-year record of millennial-scale climate variability in the North Atlantic. Science 283, 971–975.

Mischke, S., Demske, D., Wünnemann, B., Schudack, M.E., 2005. Groundwater discharge to a Gobi desert lake during Mid and Late Holocene dry periods. Palaeogeography, Palaeoclimatology, Palaeoecology 225, 157–172.

Molnar, P., Taponnier, P., 1975. Cenozoic tectonics of Asia: effects of a continental collision. Science 189, 419–426.

NorthGRIP Project Members, 2004. High-resolution record of Northern Hemisphere climate extending into the last interglacial period. Nature 431, 147–151.

Pachur, H.-J., Wünnemann, B., Zhang H., 1995. Lake evolution in the Tengger Desert, Northwestern China, during the last 40 000 years. Quaternary Research 44, 171–181.

Petit, J.R., Jouzel, J., Raynaud, D., Barkov, N.I., Barnola, J.M., Basile, I., Bender, M., Davis, M., Delaygue, G., Delmotte, M., Kotlyakov, V.M., Legrand, M., Lipenkov, V.Y., Lorius, C., Pépin, L., Ritz, C., Saltzman, E., Stievenard, M., 1999. Climate and atmospheric history of the past 420 000 years from the Vostok ice core, Antarctica. Nature 399, 429–436.

Porter, S.C., An, Z.S., 1995. Correlation between climate events in the North Atlantic and China during the last glaciation. Nature 375, 305–308.

Pye, K., Zhou, L.P., 1989. Late Pleistocene and Holocene Eolian Dust Deposition in North China and the Northwest Pacific Ocean. Palaeogeography, Palaeoclimatology, Palaeoecology 73, 11–23.

Rousseau, D.D., Wu, N., 1997. A new molluscan record of the monsoon variability over the past 130 000 yr in the Luochuan loess sequence, China. Geology 25, 275–278.

Rousseau, D.D., Antoine, P., Hatté, C., Lang, A., Zöller, L., Fontugne, M., Ben Othman, D., Luck, J.M., Moine, O., Labonne, M., Bentaleb, I., Jolly, D., 2002. Abrupt millennial climatic changes from Nussloch (Germany) Upper Weichselian eaolian records during the Last Glaciation. Quaternary Science Reviews 21, 1577–1582.

Sánchez Goñi, M.F., Eynaud, F., Turon, J.L., Shackleton, N.J., 1999. High resolution palynological record off the Iberian margin: direct land–sea correlation for the last interglacial complex. Earth and Planetary Science Letters 171, 123–137.

Sánchez Goñi, M.F., Loutre, M.F., Crucifix, M., Peyron, O., Santos, L., Duprat, J., Malaize, B., Turon, J.L., Peypouquet, J.P., 2005. Increasing vegetation and climate gradient in Western Europe over the Last Glacial Inception (122–110 ka): data-model comparison. Earth and Planetary Science Letters 231, 111–130.

Schultz, H., Rad, U.von, Erlenkeuser, H., 1998. Correlation between Arabian Sea and Greenland climate oscillations of the past 110 000 years. Nature 393, 54–57.

Shackleton, N.J., Sánchez Goñi, M.F., Pailler, D., Lancelot, Y., 2003. Marine Isotope Substage 5e and the EemianInterglacial. Global and Planetary Change 36, 151–155.

Shi Y., Yu, G., Liu, X., Li, B., Yao, T., 2001. Reconstruction of the 30–40 ka BP enhanced Indian monsoon climate based on geological records from the Tibetan Plateau. Palaeogeography, Palaeoclimatology, Palaeoecology 169, 69–83.

Sirocko, F., Seelos, K., Schaber, K., Rein, B., Dreher, F., Diehl, M., Lehne, R., Jäger, K. Krbetschek, M., Degering, D., 2005. A late Eemian aridity pulse in

central Europe during the last glacial inception. Nature 436, 833–836.

Sun, J., Ding, Z., Liu, T., 1998. Desert distributions during the glacial maximum and climatic optimum: Example of China. Episodes 21 (1), 28–30.

Thiedig, F., Oezen, D., El Chair, M., Geyh, M.A., 2000. Absolute age of the Quaternary Lacustrine Limestone of the Al Mahruqh Formation-Muzuq Basin. In: Sola, M.A., Worsley, D. (Eds.), Geological Exploration in Murzuq Basin, 89–116. Elsevier, Rotterdam.

Thompson, L.G., 2000. Ice core evidence for climate change in the Tropics: implications for our future. Quaternary Science Reviews 19, 19–35.

Thompson, L.G., Mosley-Thompson, E., Bolzan, J., Dai, N., Gundestrup, N., Yao, T., Wu, X., Klein, L., Xie, Z., 1989. Holocen/Late Pleistocene climatic ice records from Qinghai-Tibetan Plateau. Science 246, 474–477.

Thompson, L.G., Yao, T., Davis, M.E., Henderson, K. A., Mosley-Thompson, E., Lin, P.-N., Beer, J., Synal, H.A., Cole-Dai, J., Bolzan, J.F., 1997. Tropical climate instability: The last glacial cycle from a Qinghai-Tibetan ice core. Science 276, 1821–1825.

Thouveny, N., Carcaillet, J., Moreno, E., Leduc, G., Nérini, D., 2004. Geomagnetic moment variation and paleomagnetic excursions since 400 kyr BP: a stacked record from sedimentary sequences of the Portuguese margin. Earth and Planetary Science Letters 219, 377–396.

Vandenberghe, J., An, Z.S., Nugteren, G., Lu, H.Y., Huissteden, K.V., 1997. New absolute time scale for the Quaternary climate in the Chinese loess region by grain size analyses. Geology 25, 35–38.

Waelbroeck, C., Labeyrie, L., Michel, E., Duplessy, J.C., McManus, J.F., Lambeck, K., Balbon, E., Labracherie, M., 2002. Sealevel and deep water temperature changes derived from benthic foraminifera isotopic records. Quaternary Science Reviews 21, 295–305.

Wang, L., Sarnthein, M., Erlenkeuser, H., Grimalt, J., Grootes, P., Heilig, S., Ivanova, E., Kienast, M., Pelejero, C., Pflaumann, U., 1999. East Asian monsoon climate during the Late Pleistocene: high-resolution sediment records from the South China Sea. Marine Geology 156, 245–284.

Wünnemann, B., 1999. Untersuchungen zur Paläohydrographie der Endseen in der Badain Jaran- und Tengger Wüste, Innere Mongolei, Northwest-China. Habilitation thesis, Berlin, 236 pp.

Wünnemann, B., Hartmann, K., 2002. Morphodynamics and Paleohydrography of the Gaxun Nur Basin, Inner Mongolia, China. Zeitschrift für Geomorphologie. N.F., Suppl.-Bd. 126, 147–168.

Wünnemann, B., Pachur, H.-J., Zhang H., 1998. Climatic and environmental changes in the deserts of Inner Mongolia, China, since the Late Pleistocene. In: Alsharhan, A.S., Glennie, K.W., Whittle, G.L., Kendall, C.G. St. C. (Eds.), Quaternary Deserts and Climatic Change, 381–394. Balkema, Rotterdam.

Xiao, J., Porter, S.C., An, Z., Kumai, H., Yoshikawa, S., 1995. Grain size of quartz as an indicator of winter monsoon strength on the loess plateau of Central China during the last 130 000 yr. Quaternary Research 43, 22–29.

Yan, Z., Petit-Maire, N., 1994. The last 140 ka in the Afro-Asian arid/semi-arid transitional zone. Palaeogeography, Palaeoclimatology, Palaeoecology 110, 217–233.

Yang, Z., 1991. Evolution of Eastern Shelf of China in Quaternary and its environmental consequences. In: Liang, M., Zhang, J. (Eds.), Correlation of Onshore Quaternary in China, 1–22. Science Press, Beijing (in Chinese, english abstract).

Zhang, H.C., Ma, Y.Z., Li, J.J., Qi, Y., Chen, G.J., Fang, H.B., Wünnemann, B., Pachur, H.J., 2001. Palaeolake evolution and abrupt climate changes during last glacial period in NW China. Geophysical Research Letters 28 (16), 3202–3206.

Zhang, H., Wünnemann, B., Ma, Y.Z., Peng, J., Pachur, H.-J., Li J., Qi, Y., Chen, G., Fang, H., Feng, Z., 2002. Lake Leveland Climate Change between 40 000 and 18 000 14C Years BP in Tengger Desert, NW China. Quaternary Research 58, 62–72.

Zhang, H.C., Peng, J.L., Ma, Y.Z., Chen, G.J., Feng, Z.D., Li, B., Fan, H.F., Chang, F.Q., Lei, G.L., Wünnemann, B., 2004. Late Quaternary palaeolake levels in Tengger Desert, NW China. Palaeogeography, Palaeoclimatology, Palaeoecology 211, 45–58.